Journal of Power Sources 196 (2011) 3916–3920

Contents lists available at ScienceDirect

Journal of Power Sources

journal homepage: www.elsevier.com/locate/jpowsour

Short communication

Preparation of Co–Sn alloy film as negative electrode for lithium secondary batteries by pulse electrodeposition method

Koichi Ui*, Shinei Kikuchi, Yasuhiro Jimba, Naoaki Kumagai

Department of Frontier Materials and Functional Engineering, Graduate School of Engineering, Iwate University, 4-3-5 Ueda, Morioka, Iwate 020-8551, Japan

ARTICLE INFO

Article history:
Received 31 August 2010
Received in revised form
19 November 2010
Accepted 7 December 2010
Available online 23 December 2010

Keywords:
Lithium secondary battery
Negative electrode
Tin–cobalt alloy
Pulse electrodeposition

ABSTRACT

In order to easily and simply improve the cyclability of the Sn film negative electrode, we selected Co as a matrix metal and tried to prepare the Co–Sn alloy film negative electrode by a pulse electrodeposition method. The surface morphology of the deposit was almost the same as that of the Sn film, although aggregation partially occurred. The content rate of Co and Sn in the deposit was almost the same as the composition percentage in the electrodeposition bath. X-ray diffraction measurement showed that the deposited film could be assigned to a metastable Co–Sn alloy, while the co-deposition of crystalline Sn was not observed. The galvanostatic charge–discharge tests indicated that the discharge capacity and the charge–discharge efficiency of the $Co_{30.5}Sn_{69.5}$ alloy film electrode at the 1st cycle were 529.2 mAh g^{-1} and 87.9%, respectively. Furthermore, the film electrode showed a good cyclability and discharge capacity of 470.5–617.5 mAh g^{-1} during 50 cyclings. Alloying Sn with inactive Co could effectively improve the cyclability of the Sn film electrode prepared by the pulse electrodeposition method.

1. Introduction

Lithium-ion secondary batteries have been widely used as a power supply for portable devices. New functions of such devices have required an increase in energy. Although graphite (372 mAh g^{-1}) is mainly used as the negative electrode material for lithium-ion secondary batteries, Sn having about 2.5 times of the theoretical capacity (994 mAh g^{-1}) of graphite is expected as an alternative negative material. However, one of the reasons why the pure Sn electrode is not put to practical use is that its cyclability is poor. This mechanism has been generally considered as follows: the huge volume change in the host material during uptake and removal of Li is responsible for extended "cracking", "crumbling", and "pulverization" of the active material upon repeated cycling. In addition, it would undergo a loss of electrical contact with the current collector after a few cycles, leading to early exfoliation from it [1].

In order to solve these problems, the preparation of the Sn film electrode by an electrodeposition method [2], the binary alloys, such as the Sn-M alloy (M = Ni, Cu, Co, etc.) [3–5], and the structural regulation type alloy electrode aiming to increase the electrode surface area [6] have been widely reported. In the case of the Co–Sn alloy, Tamura et al. reported that the discharge capacity of the 92.1Sn–7.9Co alloy film electrode by an electroplated method was maintained with ca. 400 mAh g^{-1} after the 20th cycle [5]. Ke et al. reported the Co–Sn alloy plated film consisting of Sn and $CoSn_2$ on a porous current collector [7]. Although Sn particles are generally aggregated with increasing the cycle number, Tabuchi et al. controlled the aggregation using Co as a matrix. The discharge capacity at the 1st cycle was 561 mAh g^{-1}, but it decreased to less than 400 mAh g^{-1} after the 20th cycle [8]. To the best of our knowledge, the cyclability of many Sn alloy electrodes has not yet been accomplished compared to that of the graphite electrode. As for the Sn binary alloy film electrodes, it seems difficult to constantly maintain a capacity of more than 450 mAh g^{-1} during long-term cyclings [9].

On the other hand, we prepared a Sn film electrode using a constant current electrodeposition method, but it did not show a good cyclability. To easily and simply improve the cyclability of the Sn film electrode, we have selected a constant current pulse electrodeposition method because it is easy to accurately control the element content of the alloy [10] and obtain uniform and fine crystal grains [11]. Moreover, due to its high surface area and short ion diffusion length, it is well known that an electrode would show a good kinetic behavior. As a result, the initial cycle performance of the Sn film prepared by the pulse electrodeposition method was significantly better than that of the Sn film prepared by the constant current electrodeposition method [11]. However, it gradually faded after the 11th cycle.

In this study, we prepared the Co–Sn alloy film electrode using inactive Co against Li, and then tried a further improvement in the cyclability of the Sn-based film electrode. We selected Co as

* Corresponding author. Tel.: +81 19 621 6340; fax: +81 19 621 6314.
E-mail address: kui@iwate-u.ac.jp (K. Ui).

0378-7753/$ – see front matter © 2010 Elsevier B.V. All rights reserved.
doi:10.1016/j.jpowsour.2010.12.002

Table 1
Composition of the electrodeposition bath for the Co–Sn alloy film.

Components	Concentration (mmol dm^{-3})
$SnCl_2{\cdot}2H_2O$	175
$CoCl_2{\cdot}6H_2O$	75.0
$Na_4P_2O_7{\cdot}10H_2O$	500
Glycine	250
NH_4OH	8.25×10^{-3}

a matrix metal because of the following features: The electrical conductivity of Co (16.0×10^4 S cm^{-1}) is higher than that of Sn (9.1×10^4 S cm^{-1}), and the SHE values of Co (−0.277 V) and Sn (−0.138 V) are comparatively close for the electrodeposition preparation of the binary alloy.

2. Experimental

The composition of the electrodeposition bath is shown in Table 1. It was prepared using $SnCl_2{\cdot}2H_2O$ (Kanto Chemical Co., 96.0%) and $CoCl_2{\cdot}6H_2O$ (Kanto Chemical Co., 99.0%) as the sources of Sn and Co, respectively. The Co–Sn alloy film was prepared on one side of a nickel foil (Nilaco Co., 99.9%, 0.15 mm thickness) in the bath using a pulse electrodeposition method. The conditions of the pulse electrodeposition method were as follows: a bath temperature of 50 °C, a current density of 76 mA cm^{-2}, a pulse period of 5.0 s, a pulse of duty ratio of 0.2, a deposition time of 2.0 min, and an electricity of 1.824 C cm^{-2}.

The characterization and the surface observation of the electrodeposited films were examined by X-ray diffraction (XRD) using an X-ray diffraction meter (Rigaku Denki, RINT2200, AFC-7) with CuKα radiation (λ = 0.15418 nm), scanning electron microscopy (JEOL, JSM-7001F, FE-SEM), energy dispersive X-ray spectroscopy (OXFORD, INCA, EDX), and atomic force microscopy (Veeco, Dimension 3000, AFM). A digimicro (Nikon, MF-501) was used for the measurement of the film thickness.

A three-electrode cell was used for the electrode characteristics evaluation. The electrodeposited Co–Sn alloy film (W.E.), Li foils (R.E. and C.E.), and a 1 mol dm^{-3} solution of $LiClO_4$/EC + DEC (50:50 vol.%) (Mitsubishi Chemical Co.; water content under 30 ppm) were used for the electrochemical measurements. Cyclic voltammetry (Hokuto Denko, HZ-5000, CV) and the galvanostatic charge–discharge test (Hokuto Denko, HJR-1010mSM8) were used for the electrochemical measurements. The CVs were measured at the scan rate of 0.1 mV s^{-1} between the potentials of 0.02 and 2.00 V (vs. Li/Li$^+$). The charge–discharge tests were measured at the current density of 198 mA g^{-1} (0.2*C* rate, 1*C* = 994 mA g^{-1}) between 0.02 and 1.5 V.

Table 2
Composition of the electrodeposition bath and the Co–Sn alloy film determined by EDX spectroscopy.

	Co	Sn
Composition of electrodeposition bath (mol%)	30.0	70.0
Composition of deposit (at.%)	30.5	69.5

3. Results and discussion

The current efficiency, the amount, and the film thickness of the deposit obtained from the electrodeposition bath with the mole percentage of Co and Sn of 30:70 were 88.0%, 0.83 mg cm^{-2}, and ca. 1.10 μm, respectively. Fig. 1 shows an SEM image and the element mappings of the deposit. The crystal grain size was less than 0.5 μm, which was a little small compared to that of the Sn film (ca. 1.0 μm) [11]. In addition, partial aggregation of deposited particles was observed, which may influence the roughness of the deposit. From the mappings, both Sn and Co were found to uniformly exist on the film surface.

In order to further investigate the surface morphology, the AFM images of (a) the Sn film and (b) the deposit were observed (Fig. 2). The arithmetic values (Ra) of the Sn film and the deposit were 0.324 μm and 0.361 μm, respectively, showing that the roughness of the deposit film slightly increased due to the aggregation during electrodeposition. However, the surface morphologies of the Sn film and the deposit were similar.

The compositions of Co and Sn in the deposit obtained by EDX are shown in Table 2. The contents of Co and Sn were almost the same as the composition of the electrodeposition bath. This reveals that the element content rate of the alloy film can be controlled by adjusting the composition of the electrodeposition bath. Thereafter, the chemical formula of this film is denoted as $Co_{30.5}Sn_{69.5}$.

Fig. 3 shows the SEM image of a cross-section view and the element mappings of the deposit. From the cross-section view, the film thickness was about 1 μm. This value was almost in agreement with the value measured by AFM. From the mappings, it is observed that the deposit composition is homogenous along in the depth direction.

The XRD pattern of the $Co_{30.5}Sn_{69.5}$ alloy film is shown in Fig. 4. Because the XRD pattern of the $Co_{30.5}Sn_{69.5}$ alloy film consisted of several broad peaks, it would be a metastable phase. In addition, crystalline Sn was not detected because the main peaks at 32°, 44°, and 45° were not attributed to Sn. Moreover, the observed XRD peaks were not attributed to some Co–Sn alloy components such as Co_3Sn_2 (JCPDS no. 02-0724), CoSn (JCPDS no. 02-0559), $CoSn_2$ (JCPDS no. 25-0256), and α-$CoSn_3$ (JCPDS no. 48-1813). On the other hand, Tamura et al. reported that the 79.8Sn–20.2Co alloy film was the amorphous Co–Sn alloy having two broad peaks around 32°, 43° [12]. In this case, the possibility including amorphous Sn was not suggested. Based on the above, it is considered that the

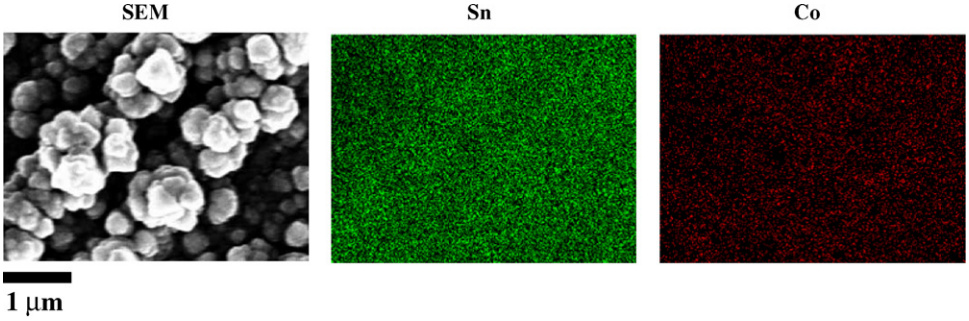

Fig. 1. SEM image of film deposit prepared by the constant current pulse electrodeposition method and corresponding EDX mappings for the Sn and Co elements; bath temperature: 50 °C; current density: 76 mA cm^{-2}; pulse period: 5.0 s; pulse duty ratio: 0.2; deposition time: 2.0 min; electricity: 1.824 C cm^{-2}.

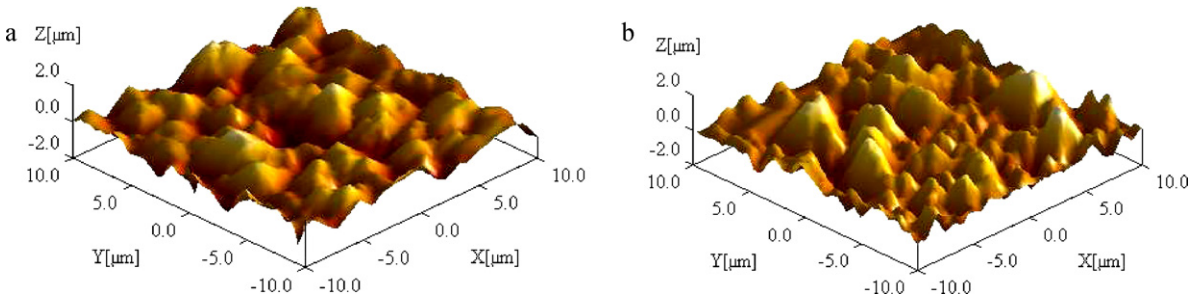

Fig. 2. AFM images of (a) Sn film and (b) the deposit film prepared by the constant current pulse electrodeposition method.

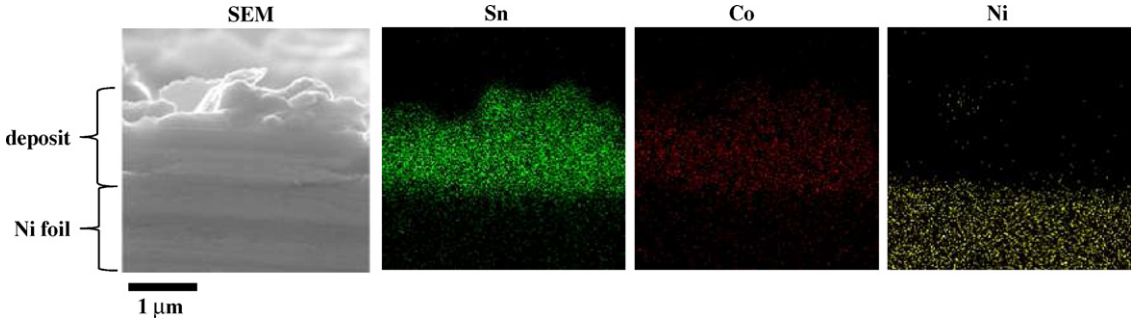

Fig. 3. SEM image of the cross-section view of the deposit prepared by the constant current pulse electrodeposition method and corresponding EDX mappings for the elements Sn, Co, and Ni.

$Co_{30.5}Sn_{69.5}$ alloy film would be a metastable phase not including crystalline Sn.

The CVs were measured in order to investigate the electrochemical behavior of the $Co_{30.5}Sn_{69.5}$ alloy film electrode (Fig. 5). As seen in the figure, the reduction peak in the potential at 0.2 V is assumed to be due to the electrochemical reaction of Sn component in the Co_ySn alloy involving the formation of the Li_xSn alloy and the separation of Co according to Eq. (1) [13,14]. In contrast, the oxidation peaks corresponding to the reduction peak at 0.20 V were observed at 0.50 and 0.70 V. These peaks may be due to a dealloying reaction from Li_xSn to form Li and Sn according to Eq. (2) [15,16].

$$Co_ySn + xLi^+ + xe^- \rightarrow Li_xSn + yCo \quad (0 < x < 4.4) \tag{1}$$

$$Li_xSn + yCo \rightarrow Sn + xLi^+ + yCo + xe^- \tag{2}$$

The reduction peak at the 2nd cycle clearly shifted from 0.20 V to 0.30 V, indicating that Sn separated from the Co–Sn alloy during the initial cycling would react with Li during following cycling. These results suggested that the Sn component would be isolated from the $Co_{30.5}Sn_{69.5}$ alloy during the 1st cycle as shown in Eq. (2), and then isolated Sn would react with Li at the 2nd cycle [17]. Moreover, for the Sn film electrode prepared by the pulse electrodeposition method, the small reduction wave was observed

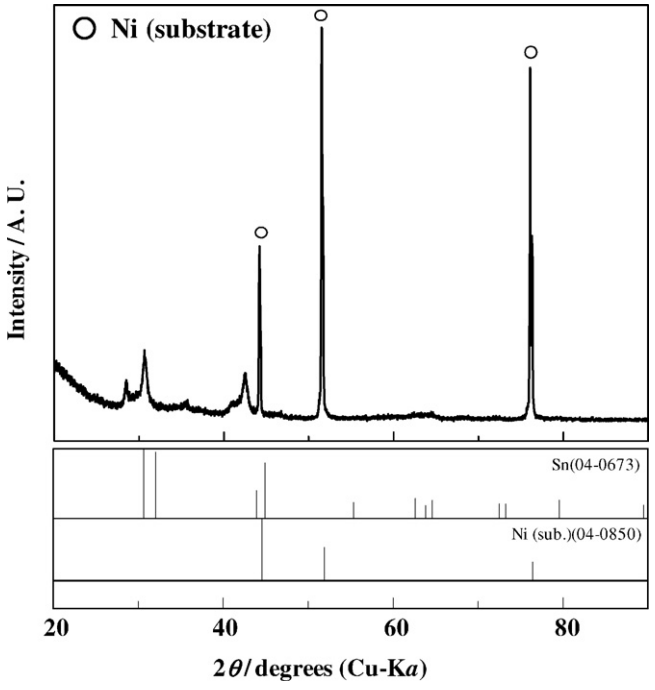

Fig. 4. XRD pattern of $Co_{30.5}Sn_{69.5}$ alloy film prepared by the constant current pulse electrodeposition method.

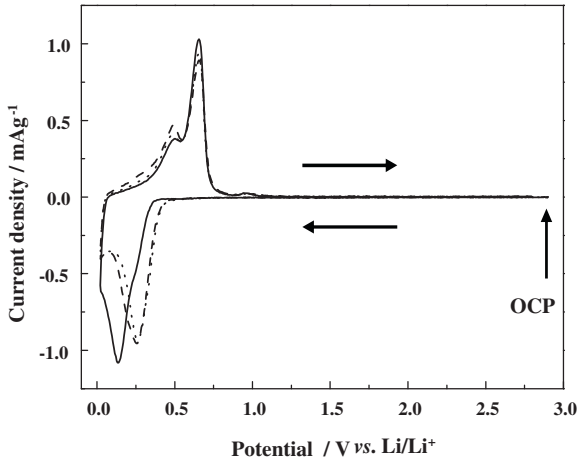

Fig. 5. Cyclic voltammograms of $Co_{30.5}Sn_{69.5}$ alloy film electrode prepared by the constant current pulse electrodeposition method; potential range: 0.02–2.00 V vs. Li/Li^+, scan rate: 0.1 mV s^{-1}; (––) 1st cycle; (- - -) 2nd cycle; (...) 3rd cycle.

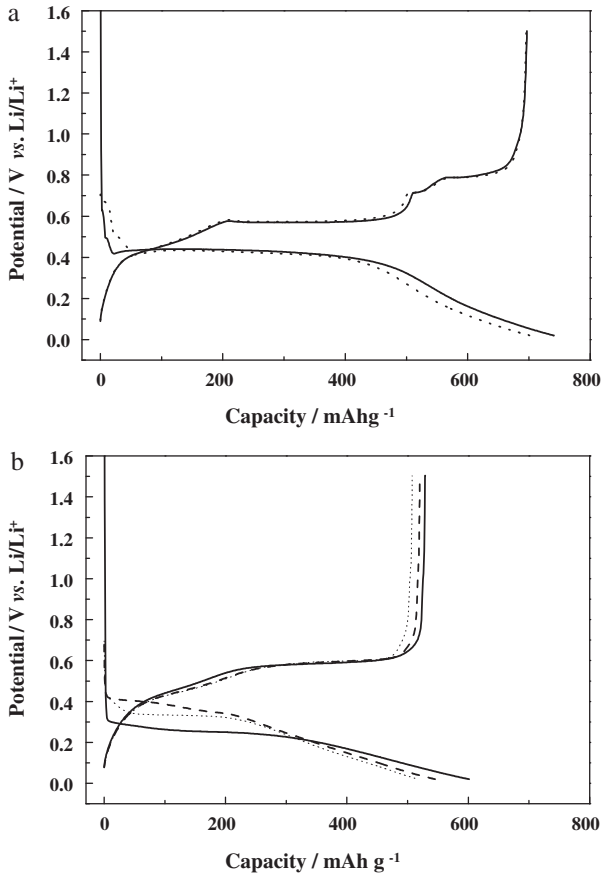

Fig. 6. Charge–discharge curves of (a) Sn film electrode [11] and (b) $Co_{30.5}Sn_{69.5}$ alloy film electrode; potential range: 0.02–1.50 V vs. Li/Li^+, C.D.: 198 mA g^{-1} (0.2*C*); (––) 1st cycle; (- - -) 2nd cycle; (. . .) 3rd cycle.

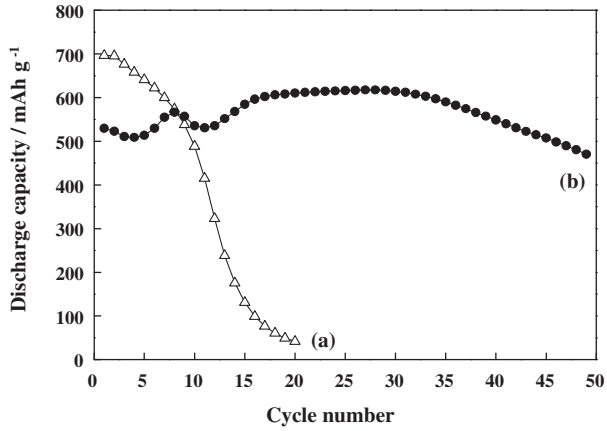

Fig. 7. Cycle performance of (a) Sn and (b) $Co_{30.5}Sn_{69.5}$ alloy film electrodes; potential range: 0.02–1.50 V vs. Li/Li^+, C.D.: 198 mA g^{-1} (0.2*C*).

at ca. 1.6 V in our previous paper [11]. This wave may be due to the reduction of SnO_x or the decomposition of the electrolyte. For the $Co_{30.5}Sn_{69.5}$ alloy film electrode, however, such a reduction wave is not observed at the potential around 1.5 V as seen in Fig. 5.

Fig. 6 shows the charge–discharge curves of (a) the Sn film electrode [11] and (b) the $Co_{30.5}Sn_{69.5}$ alloy film electrode at the current density of 198 mA g^{-1}(0.2*C*). The discharge capacity and the charge–discharge efficiency of the $Co_{30.5}Sn_{69.5}$ alloy film electrode at the 1st cycle were 529.2 mAh g^{-1} and 87.9%, respectively. The discharge capacity at the 1st cycle of the $Co_{30.5}Sn_{69.5}$ alloy film electrode was lower than that of the Sn film electrode (696.8 mAh g^{-1}) [11], indicating that the Co component would not participate in the charge–discharge reaction because Co does not electrochemically react with Li. The potential profile of the $Co_{30.5}Sn_{69.5}$ alloy film electrode was similar to that of the Sn film electrode after the 2nd cycle, although that of the $Co_{30.5}Sn_{69.5}$ alloy film electrode at the 1st cycle was different from that of the Sn film electrode. These results almost corresponded to those of the CV measurements.

The cycle performances of (a) the Sn film electrode and (b) the $Co_{30.5}Sn_{69.5}$ alloy film electrode are shown in Fig. 7. Although the discharge capacity of the Sn film electrode at the 1st cycle was a very high value of 696.8 mAh g^{-1} [11], a gradual capacity fade occurred during 10–20 cyclings (a). This result indicates that exfoliation of the Sn film could not be sufficiently suppressed only by reducing the crystal grain size. In contrast, such a rapid decrease in capacity was not observed in the subsequent cycle for the $Co_{30.5}Sn_{69.5}$ alloy (b). It should be noted that a high discharge capacity of the $Co_{30.5}Sn_{69.5}$ alloy film electrode was obtained with 470.5 mAh g^{-1} after the 50th cycle, although the discharge capacity of the $Co_{30.5}Sn_{69.5}$ alloy film electrode at the 1st cycle was lower than that of the Sn film electrode. It was previously reported that inactive Co matrix would prevent the aggregation during cycling although Sn tends to aggregate resulting in volume change and capacity decay [8]. We may, therefore, reasonably consider that the volume change of Sn would be restrained and then the exfoliation of the alloy film from the current collector would be reduced by alloying with Co.

Based on the results, it seems to be concluded that alloying Sn with different metals would effectively improve the cyclability of the Sn film electrode. In addition to these results, we will report the effect of the composition of the alloy film on the electrode characteristics in the near future.

4. Conclusion

To easily and simply improve the cyclability of the Sn film negative electrode, we prepared the Co–Sn alloy film electrode by a pulse electrodeposition method and obtained the following results. An obvious difference appeared in the cyclability by adding Co as a matrix metal to the Sn film, although the surface morphology and the thickness of the deposit were almost the same as those of the Sn film prepared by the pulse electrodeposition method. By controlling the composition of the electrodeposition bath, the compositions of the alloy film could be controlled, and in the alloy film both Co and Sn components were uniformly dispersed. The cycle performance of the $Co_{30.5}Sn_{69.5}$ alloy film electrode was much better than that of the Sn film electrode. The discharge capacity of the $Co_{30.5}Sn_{69.5}$ alloy film electrode was maintained with 470.5 mAh g^{-1} after the 50 cycles. The volume change of the film electrode during cyclings may be restrained by alloying Sn with Co, and the exfoliation of the film from the current collector would be reduced. Moreover, the Co–Sn alloy film not containing crystalline Sn prepared by pulse electrodeposition method would lead to an improvement in the cyclability.

References

[1] M. Wachtler, J.O. Besenhard, M. Winter, J. Power Sources 94 (2001) 189.
[2] H. Morimoto, S. Tobishima, H. Negishi, J. Power Sources 146 (2005) 469.
[3] W. Pu, X. He, J. Ren, C. Wan, C. Jiang, Electrochim. Acta 50 (2005) 4140.
[4] J. Hassoun, S. Panero, B. Scrosati, J. Power Sources 160 (2006) 1336.
[5] N. Tamura, Y. Kato, A. Mikami, M. Kamino, S. Matsuta, S. Fujitani, J. Electrochem. Soc. 153 (2006) A2227.
[6] K. Nishikawa, K. Dokko, K. Kinoshita, S.W. Woo, K. Kanamura, J. Power Sources 189 (2009) 726.

[7] F.S. Ke, L. Huang, H.B. Wei, J.S. Cai, X.Y. Fan, F.Z. Yang, S.G. Sun, J. Power Sources 170 (2007) 450.
[8] T. Tabuchi, N. Hochgatterer, Z. Ogumi, M. Winter, J. Power Sources 188 (2009) 552.
[9] X.Y. Fan, F.S. Ke, G.Z. Wei, L. Huang, S.G. Sun, J. Alloys Compd. 476 (2009) 70.
[10] S.D. Beattie, J.R. Dahn, J. Electrochem. Soc. 150 (2003) A894.
[11] K. Ui, S. Kikuchi, Y. Kadoma, N. Kumagai, S. Ito, J. Power Sources 189 (2009) 224.
[12] N. Tamura, M. Fujimoto, M. Kamino, S. Fujitani, Electrochim. Acta 49 (2004) 1949.
[13] I. Amadei, S. Panero, B. Scrosati, G. Cocco, L. Schiffini, J. Power Sources 143 (2005) 227.
[14] J.J. Zhang, Y.Y. Xia, J. Electrochem. Soc. 153 (2006) A1466.
[15] M. Winter, J.O. Besenhard, Electrochim. Acta 45 (1999) 31.
[16] R.A. Huggins, J. Power Sources 81–82 (1999) 13.
[17] T. Sonoda, T. Sakai, J. Surf. Finish. Soc. Jpn. 54 (2003) 492.